

Constraining Non-Standard Interactions of the Neutrino with Borexino

Sanjib Kumar Agarwalla,^a Francesco Lombardi,^b and Tatsu Takeuchi^c

^a*Instituto de Física Corpuscular, CSIC-Universitat de València, Apartado de Correos 22085, E-46071 Valencia, Spain*

^b*Università degli Studi dell'Aquila, Dipartimento di Fisica, L'Aquila, Italy and INFN, Laboratori Nazionali del Gran Sasso, Assergi (AQ), Italy*

^c*Center for Neutrino Physics, Physics Department, Virginia Tech, Blacksburg, 24061 VA, USA*
E-mail: Sanjib.Agarwalla@ific.uv.es, francesco.lombardi@lngs.infn.it, takeuchi@vt.edu

ABSTRACT: We use the Borexino 153.6 ton·year data to place constraints on non-standard neutrino-electron interactions, taking into account the uncertainties in the ${}^7\text{Be}$ solar neutrino flux and the mixing angle θ_{23} , and backgrounds due to ${}^{85}\text{Kr}$ and ${}^{210}\text{Bi}$ β -decay. We find that the bounds are comparable to existing bounds from all other experiments. Further improvement can be expected in Phase II of Borexino due to the reduction in the ${}^{85}\text{Kr}$ background.

KEYWORDS: Neutrino, Borexino, Non-Standard Interactions

ARXIV EPRINT: [1207.3492](https://arxiv.org/abs/1207.3492)

We dedicate this paper to the memory of Raju Raghavan who played a significant role in the Borexino experiment and was the initiator and driving force behind this work.

Contents

1	Introduction	1
2	Neutrino-Electron Elastic Scattering	3
3	The Borexino Detector and beta-decay Backgrounds	5
4	Uncertainty in the Standard Solar Model Neutrino Flux Prediction	7
5	Uncertainties in the Mixing Angles	8
6	Dependence of the Event Spectrum on the NSI Parameters	9
7	Analysis Results	11
7.1	Method of Analysis	11
7.2	One NSI parameter at a time limits	12
7.3	Constraints in the $(\varepsilon_{eL}-\varepsilon_{eR})$ and $(\varepsilon_{\tau L}-\varepsilon_{\tau R})$ planes	14
8	Summary	15

1 Introduction

Various extensions of the Standard Model (SM), such as left-right symmetric models and supersymmetric models with R-parity violation, predict non-standard interactions (NSIs) of the neutrinos with other fermions [1–11]. The NSIs in those models are generated via the exchange of new massive particles and at low-energies can be described by effective four fermion interactions of the form

$$\mathcal{L}_{\text{NSI}} = -2\sqrt{2}G_F\varepsilon_{\alpha\beta}^{ff'C}(\bar{\nu}_\alpha\gamma^\mu P_L\nu_\beta)(\bar{f}\gamma_\mu P_C f'), \quad (1.1)$$

where G_F is the Fermi constant, α and β are neutrino flavor indices, f and f' label light SM fermions, $C = L$ or R is the chirality of the projection operator P_C , where $P_{L/R} = (1\mp\gamma_5)/2$, and the dimensionless number $\varepsilon_{\alpha\beta}^{ff'C}$ parametrizes the strength of the interaction.

In a previous publication from 2002 [12], Raghavan, together with Berezhiani and Rossi, discussed the potential of the Borexino detector in placing constraints on the flavor-diagonal NSI parameters

$$\varepsilon_{\alpha L} \equiv \varepsilon_{\alpha\alpha}^{eeL}, \quad \varepsilon_{\alpha R} \equiv \varepsilon_{\alpha\alpha}^{eeR}, \quad \alpha = e \text{ or } \tau, \quad (1.2)$$

via the measurement of the electron recoil spectrum in $\nu_\alpha e$ elastic scattering. There, it was argued that due to the mono-energetic nature of the ${}^7\text{Be}$ solar neutrinos, Borexino

would be able to place stronger constraints on ε_{eR} and $\varepsilon_{\tau R}$ than would be possible at Super-Kamiokande (SK) and the Sudbury Neutrino Observatory (SNO) where the observed neutrinos are the ^8B neutrinos with a continuous energy spectrum.¹ The $\alpha = \mu$ case was not considered since the couplings $\varepsilon_{\mu L}$ and $\varepsilon_{\mu R}$ were already constrained to the level of $|\varepsilon_{\mu L/R}| < 0.03$ (at 90% C.L.) [14] by the $\nu_\mu e$ scattering experiment CHARM II [15].

Today, a decade later, with the Borexino experiment running smoothly and having accumulated more than 153.6 ton·years of data, it is now possible to actually extract the constraints on the flavor-diagonal NSI parameters discussed by Raghavan et al. Constraints on the same parameters from various other experiments are also available for comparison, some of which are quite new. Bounds from the solar neutrino experiments (SK, SNO, etc.) and KamLAND can be found in Refs. [14], [16], and [17]. Bounds from reactor and accelerator experiments have been compiled in Ref. [18], which includes the bounds from $e^+e^- \rightarrow \nu\bar{\nu}\gamma$ measured at LEP [19], $\nu_e e$ scattering measured at LSND [20], and $\bar{\nu}_e e$ scattering measured at the reactor experiments Irvine [21], Rovno [22], and MUNU [23]. See also Refs. [24, 25]. Bounds have also been placed using atmospheric neutrinos [26] and MINOS [27]. New bounds from the TEXONO reactor neutrino experiment can be found in Ref. [28].

In this paper, we place constraints on the NSI parameters $\varepsilon_{eL/R}$ and $\varepsilon_{\tau L/R}$ using the Borexino 153.6 ton·year data. We include in our analysis the uncertainties in the ^7Be solar neutrino flux and in the mixing angle θ_{23} , and backgrounds from ^{85}Kr and ^{210}Bi β -decay. Taking these systematic uncertainties and backgrounds into account are particularly important since they can mimic non-zero values of the parameters in question. Indeed, as will be discussed in detail in the following, we find that unless the solar-neutrino flux-uncertainty and the ^{85}Kr β -decay background are reduced, increased statistics will not improve the bounds beyond what can be extracted from current Borexino data. The parameters $\varepsilon_{\mu L/R}$ are not considered since the CHARM II bound still stands.

This paper is organized as follows. In section 2, we discuss how the electron recoil spectrum in $\nu_\alpha e$ scattering can be used to constrain the parameters $\varepsilon_{\alpha L/R}$, ($\alpha = e$ or τ) and how the above mentioned systematic uncertainties and β -decay backgrounds can interfere with the extraction. Section 3 discusses how well systematic uncertainties and backgrounds are understood in the Borexino experiment, section 4 discusses the uncertainty in the ^7Be neutrino flux in the Standard Solar Model, and section 5 discusses the uncertainties in the neutrino oscillation probabilities which depend on our knowledge of the mixing angles θ_{12} and θ_{23} . In Section 6 we look at the dependence of the electron recoil spectrum on the NSI parameters and backgrounds in detail, and how one can mimic the other. Results of our fit are presented in section 7, and section 8 concludes.

¹This possibility had been suggested earlier by Berezhiani and Rossi in Ref. [13].

2 Neutrino-Electron Elastic Scattering

In the SM, the interaction between neutrino flavor α ($\alpha = e, \mu, \tau$) and the electron is described at low energies by the effective four fermion interaction

$$\mathcal{L}_{\text{SM}} = -2\sqrt{2}G_F(\bar{\nu}_\alpha\gamma^\mu P_L\nu_\alpha)\left[g_{\alpha L}(\bar{e}\gamma_\mu P_L e) + g_{\alpha R}(\bar{e}\gamma_\mu P_R e)\right]. \quad (2.1)$$

The coupling constants at tree level are given by $g_{\alpha R} = \sin^2\theta_W$ and $g_{\alpha L} = \sin^2\theta_W \pm \frac{1}{2}$, where the lower sign applies for $\alpha = \mu$ and τ (from Z exchange only) and the upper sign applies for $\alpha = e$ (from both Z and W exchange). Radiative corrections are small and can be ignored.²

The presence of flavor-diagonal NSIs, $\varepsilon_{\alpha L/R}$, will shift the coupling constants in the above expression to

$$g_{\alpha L} \rightarrow \tilde{g}_{\alpha L} = g_{\alpha L} + \varepsilon_{\alpha L}, \quad g_{\alpha R} \rightarrow \tilde{g}_{\alpha R} = g_{\alpha R} + \varepsilon_{\alpha R}. \quad (2.2)$$

This interaction between electron and neutrino, with possible shifts in the coupling constants, can be observed via the elastic scattering of a neutrino of flavor α off of an electron at rest, which has the differential cross section [31]

$$\frac{d\tilde{\sigma}_{\nu_\alpha}(E_{\nu_\alpha}, T)}{dT} = \frac{2G_F^2 m_e}{\pi} \left[\tilde{g}_{\alpha L}^2 + \tilde{g}_{\alpha R}^2 \left(1 - \frac{T}{E_{\nu_\alpha}}\right)^2 - \tilde{g}_{\alpha L}\tilde{g}_{\alpha R} \frac{m_e T}{E_{\nu_\alpha}^2} \right]. \quad (2.3)$$

Here, m_e is the electron mass, E_{ν_α} is the initial neutrino energy, and T is the kinetic energy of the recoil electron which has the range

$$0 \leq T \leq T_{\text{max}} = \frac{E_{\nu_\alpha}}{1 + m_e/2E_{\nu_\alpha}}. \quad (2.4)$$

If the incoming neutrino beam is mono-energetic, no convolution of Eq. (2.3) with the neutrino energy spectrum is necessary.

The ${}^7\text{Be}$ solar neutrinos are produced via the K-shell electron capture processes [32]

$${}^7\text{Be} + e^- \rightarrow \begin{cases} {}^7\text{Li} + \nu_e & (89.6\%), \\ {}^7\text{Li}^*(0.48) + \nu_e & (10.4\%), \end{cases} \quad (2.5)$$

yielding mono-energetic neutrinos of energy 0.862 MeV and 0.384 MeV, respectively. Borexino is sensitive to the 0.862 MeV component, for which the maximum recoil energy is

²In the notation of Ref. [29], the coupling constants for the $\alpha = \mu$ case, including radiative corrections, are expressed as

$$g_{\mu L} = \frac{g_V^{\nu e} + g_A^{\nu e}}{2} = \rho_{\nu e} \left(-\frac{1}{2} + \hat{\kappa}_{\nu e} \hat{s}_Z^2 \right), \quad g_{\mu R} = \frac{g_V^{\nu e} - g_A^{\nu e}}{2} = \rho_{\nu e} \left(-\frac{1}{2} \right),$$

where \hat{s}_Z^2 is the $\overline{\text{MS}}$ value of $\sin^2\theta_W$, and $\rho_{\nu e}$ and $\hat{\kappa}_{\nu e}$ denote process specific corrections. At zero-momentum transfer, these are $\rho_{\nu e} = 1.0128$ and $\hat{\kappa}_{\nu e} = 0.9963$ [29]. Since the deviations of these parameters from one are small compared to the sensitivity of Borexino, they, and any flavor dependence that may exist for the $\alpha = e, \tau$ cases, can be ignored. In our analysis, we use the $\overline{\text{MS}}$ value of $\hat{s}_Z^2(0.862 \text{ MeV}) = 0.2386$ [30] for $\sin^2\theta_W$, and the tree-level expressions for the couplings.

$T_{\max} = 0.665$ MeV. This component arrives at the Earth as a superposition of the three neutrino flavors due to the MSW effect and vacuum oscillation. If we denote the survival probability of ν_e in this component at the Borexino detector as P_{ee} , then the total neutrino-electron scattering cross section there will be the combination

$$\frac{d\tilde{\sigma}_\nu(T)}{dT} = \left[P_{ee} \frac{d\tilde{\sigma}_{\nu_e}(T)}{dT} + (1 - P_{ee}) \left(c_{23}^2 \frac{d\tilde{\sigma}_{\nu_\mu}(T)}{dT} + s_{23}^2 \frac{d\tilde{\sigma}_{\nu_\tau}(T)}{dT} \right) \right], \quad (2.6)$$

where $c_{23}^2 = \cos^2 \theta_{23}$ and $s_{23}^2 = \sin^2 \theta_{23}$. Thus, the measurement of the T -dependence of the ${}^7\text{Be}$ solar neutrino elastic scattering event rate will let us constrain the values of $\tilde{g}_{\alpha L}$ and $\tilde{g}_{\alpha R}$ for all flavors.

An actual detector, however, cannot measure the recoil electron energy to arbitrary precision, and one must take its finite energy resolution into account. If we denote the probability of detecting energy T_A for an electron with kinetic energy T by $R(T_A, T)$, the differential cross section as a function of the actual detection energy T_A is given by

$$\frac{d\bar{\sigma}_{\nu_\alpha}(T_A)}{dT_A} = \int_0^{T_{\max}} R(T_A, T) \frac{d\tilde{\sigma}_{\nu_\alpha}(T)}{dT} dT. \quad (2.7)$$

For Borexino, we take the energy resolution function $R(T_A, T)$ to be a gaussian with a T -dependent standard deviation

$$R(T_A, T) = \frac{1}{\sqrt{2\pi} \sigma(T)} \exp \left[-\frac{(T_A - T)^2}{2[\sigma(T)]^2} \right], \quad (2.8)$$

where $\sigma(T)$ is given by [33]

$$\sigma(T) = \sigma_0 \left(\frac{T}{\text{MeV}} \right)^{1/2}, \quad \sigma_0 = 50 \text{ keV}. \quad (2.9)$$

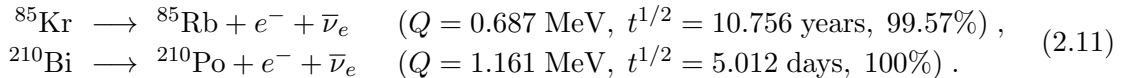
This will ‘blur-out’ the shape of the energy spectrum somewhat, smoothing out the Compton-like edge of $d\tilde{\sigma}_\nu(T)/dT$, but still retain its basic overall shape.

Thus, for an incoming 0.862 MeV ${}^7\text{Be}$ neutrino flux of $\Phi_{7\text{Be}}^{0.862}$ and number of electrons N_e in the fiducial volume of the detector, the number of recoil electrons detected with energy in the bin $T_1 < T_A < T_2$ per unit time is given by

$$\begin{aligned} \frac{dN(T_1, T_2)}{dt} &= N_e \Phi_{7\text{Be}}^{0.862} \int_{T_1}^{T_2} \frac{d\bar{\sigma}_\nu(T_A)}{dT_A} dT_A \\ &= N_e \Phi_{7\text{Be}}^{0.862} \left[P_{ee} \int_{T_1}^{T_2} \frac{d\bar{\sigma}_{\nu_e}(T_A)}{dT_A} dT_A \right. \\ &\quad \left. + (1 - P_{ee})(1 - s_{23}^2) \int_{T_1}^{T_2} \frac{d\bar{\sigma}_{\nu_\mu}(T_A)}{dT_A} dT_A \right. \\ &\quad \left. + (1 - P_{ee})s_{23}^2 \int_{T_1}^{T_2} \frac{d\bar{\sigma}_{\nu_\tau}(T_A)}{dT_A} dT_A \right]. \quad (2.10) \end{aligned}$$

By measuring this spectrum, Borexino can constrain both $\varepsilon_{eL/R}$ and $\varepsilon_{\tau L/R}$. However, the precision of those constrains will depend on the uncertainty in the prefactor $N_e \Phi_{7\text{Be}}^{0.862}$, which is still quite significant, and those in P_{ee} and s_{23}^2 .

The measurement of the recoil electron energy spectrum in Borexino is further complicated by the fact that it is impossible to distinguish between electrons from $\nu_\alpha e$ scattering and those from β -decay of radioactive nuclei. The most significant β backgrounds in Borexino are those from the decays



As will be shown later, the electrons from ${}^{85}\text{Kr}$ decay are particularly problematic. Of the decay products, ${}^{85}\text{Rb}$ is stable while ${}^{210}\text{Po}$ subsequently undergoes α -decay



This α -particle can mimic β -particles in the relevant energy range, but this particular background can be removed reliably using pulse shape analysis [34]. ${}^{206}\text{Pb}$ is stable.

In the next section, we will review the properties of the Borexino detector, and how well these β -decay backgrounds are understood.

3 The Borexino Detector and beta-decay Backgrounds

Borexino is a real-time solar neutrino detector designed to measure the 0.862 MeV monoenergetic ${}^7\text{Be}$ solar neutrinos. It is situated in Hall C of the Laboratori Nazionali del Gran Sasso (LNGS), Italy, below 1400 meters of rock (3800 meters water equivalent) where the muon flux is suppressed by a factor of $\sim 10^6$ compared to the Earth's surface. Borexino's spherical vessel is filled with ~ 278 tons of liquid scintillator (pseudocumene doped with 2,5-diphenyloxazole as a wavelength shifter), with the fiducial volume consisting of the central 100 tons. In the period from May 16, 2007 to May 8, 2010, Borexino had 740.7 live days of data taking, corresponding to 153.6 ton·years of fiducial exposure. [35–37]

The neutrinos are detected via their elastic scattering off of electrons in the scintillator. The scintillation light from the recoil electrons spread isotropically from the event location, and are detected by an array of ~ 2200 photomultiplier tubes (PMTs) mounted onto a stainless steel sphere, looking into the detector volume. A neutrino event is identified by multiple PMT hits within a Trigger Time Window (TTW) of 60 nanoseconds, with the total number of photoelectrons collected exceeding a given threshold. This triggers the recording of all PMT hits for 16 microseconds, from which the electron recoil energy T_A is reconstructed. The location of the event within the detector is determined from the difference in arrival times of the TTW photons to different parts of the PMT array. For a $T_A \sim 1$ MeV event, this system can identify its location to a precision of about 10 cm [38].

The chemical composition of pseudocumene is C_9H_{12} with atomic mass 120.19, and 66 electrons per molecule. Thus, the number of electrons within the fiducial volume of 100 tons of pseudocumene can be calculated to be $N_e = 3.307 \times 10^{31}$. However, due to the limited event-position resolution of Borexino discussed above, there exists an uncertainty in the fiducial volume of ${}_{-1.3}^{+0.5}\%$ which propagates directly into an uncertainty in N_e [37].

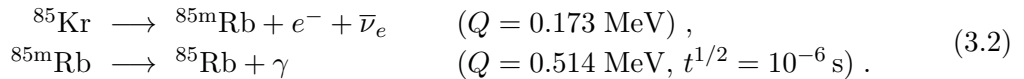
As discussed in the previous section, the electrons from ${}^{85}\text{Kr}$ and ${}^{210}\text{Bi}$ β -decay present significant backgrounds to the measurement of the ${}^7\text{Be}$ signal. Due to the Q -values of these

decays being close to the ${}^7\text{Be}$ solar neutrino energy, their β -decay spectra overlap with the ${}^7\text{Be}$ recoil electron spectrum as shown in figure 1. Of the other backgrounds present, that due to ${}^{14}\text{C}$, which β -decays with Q -value of 0.1565 MeV, is large but occupies a much lower energy range [39]. The background due to cosmogenic ${}^{11}\text{C}$ [40], which β^+ -decays with Q -value of 0.96 MeV, is at larger energies. A fit to the measured count rate assuming SM interactions yields (TABLE I of Ref. [37])

$$\begin{aligned} {}^7\text{Be} &: 46.0 \pm 1.5(\text{stat})_{-1.6}^{+1.5}(\text{syst}) \quad \text{counts}/(\text{day} \cdot 100 \text{ tons}) , \\ {}^{85}\text{Kr} &: 31.2 \pm 1.7(\text{stat}) \pm 4.7(\text{syst}) \quad \text{counts}/(\text{day} \cdot 100 \text{ tons}) , \\ {}^{210}\text{Bi} &: 41.0 \pm 1.5(\text{stat}) \pm 2.3(\text{syst}) \quad \text{counts}/(\text{day} \cdot 100 \text{ tons}) , \end{aligned} \quad (3.1)$$

showing that the count rates of the ${}^{85}\text{Kr}$ and ${}^{210}\text{Bi}$ backgrounds are of the same order of magnitude as that of the ${}^7\text{Be}$ signal. Thus, the distortions of the shape of the count rate spectrum due to these backgrounds are significant. Furthermore, the shapes of the ${}^{85}\text{Kr}$ and ${}^{210}\text{Bi}$ β -spectra are such that the said distortions are similar to those due to non-zero values of the NSI parameters. Thus, in order to extract the bounds on the NSI parameters from the count rate data, it is crucial that we can determine the ${}^{85}\text{Kr}$ and ${}^{210}\text{Bi}$ backgrounds independently.

For ${}^{85}\text{Kr}$, this is possible by utilizing the following decay chain which constitutes 0.43% of ${}^{85}\text{Kr}$ -decay :

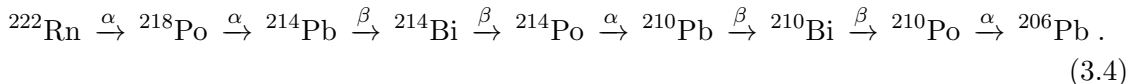


Delayed coincidence measurements of the β and γ from this decay-chain has yielded the total count rate of [41]

$${}^{85}\text{Kr} : 30.4 \pm 5.3(\text{stat}) \pm 1.3(\text{syst}) \text{ counts}/(\text{day} \cdot 100 \text{ tons}) , \quad (3.3)$$

which is consistent with the fit value listed in Eq. (3.1). We will use this direct measurement value as a constraint in our analysis.

${}^{210}\text{Bi}$ is a pure β -emitter produced at the end of the ${}^{222}\text{Rn}$ decay chain:



It was proposed in Ref. [42] that the quantity of ${}^{210}\text{Bi}$ in liquid scintillation detectors may be determined directly from the quantity of its decay product ${}^{210}\text{Po}$, which in turn can be determined by measuring its α -decay rate. Unfortunately, this method cannot be used due to temporal instabilities of the Borexino data. However, in the narrow energy range above the ${}^7\text{Be}$ shoulder and below the lower end of the ${}^{11}\text{C}$ β^+ -decay spectrum, aka the “ ${}^7\text{Be}$ valley,” the count rate is dominated by ${}^{210}\text{Bi}$ decay. The count rates from the other two components that contribute in this valley, namely the CNO and pep solar neutrinos, are too low compared to that of ${}^{210}\text{Bi}$ to be measured with statistical significance. Indeed, the contributions of CNO and pep neutrinos are small throughout the energy range of our analysis, with count rates comparable to the statistical errors of the β -decay backgrounds [43]. Therefore, though the precision is limited by statistics, fitting to the count rate in the valley can constrain the ${}^{210}\text{Bi}$ background independently of the fit to the NSI parameters.

4 Uncertainty in the Standard Solar Model Neutrino Flux Prediction

The precisions of the neutrino fluxes predicted by the Standard Solar Model (SSM) depend on the precisions of the physical input parameters. In the past, the ${}^7\text{Be}$ neutrino flux prediction suffered from a large uncertainty (12% in Ref. [44] from 2004) stemming mostly from a large uncertainty in the cross section of the reaction



at energies relevant to reactions in the Solar core. This cross section had been measured by shooting an α -beam into a gas ${}^3\text{He}$ target, and counting the number of produced ${}^7\text{Be}$ by either detecting the γ s in the above reaction (prompt method), or by measuring the amount of accumulated ${}^7\text{Be}$ later by counting the γ s from the decay of ${}^7\text{Li}^*$ (0.48) produced in the second reaction of Eq. (2.5) (activation method). The large uncertainty was due to a disagreement between the results obtained via the prompt and activation methods. Extrapolating the results down to the relevant energies lead to an additional uncertainty. In the last decade, however, these uncertainties have been reduced considerably by the LUNA experiment at the LNGS by a resolution of the discrepancy between the two methods, and the measurement of the cross section at lower energies than before [45, 46]. As a result, the error in the ${}^7\text{Be}$ neutrino flux due to this particular uncertainty has been reduced from 8% to 2.8% [47].

Unfortunately, solar metallicity has come into the picture as a new source of large uncertainty. The abundance of various elements inside the Sun is inferred from the measurements of their abundances in planets, chondrites³, and other bodies in the Solar system, and from the analysis of absorption lines in the Solar photosphere spectrum. The abundances inferred from the latter depend on the hydrodynamic model used for the photosphere. A determination based on a 1D model of the solar atmosphere published in 1998 [48] (GS98) has been used as input to the SSM for many years. A new determination based on a state-of-the-art 3D model, and other improvements, was published in 2009 [49] (AGSS09). The inferred values of the metallicity at the solar surface is $(Z/X)_\odot = 0.0229$ in GS98, but $(Z/X)_\odot = 0.0178$ in AGSS09.⁴ The SSM predictions of the total ${}^7\text{Be}$ neutrino flux (sum of the 0.862 MeV and 0.384 MeV components) for the two cases are [50]

$$\begin{aligned} \Phi_{7\text{Be}}^{\text{total}} &= 5.00 (1 \pm 0.07) \times 10^9 \text{ cm}^{-2}\text{s}^{-1} && \text{(GS98)}, \\ &= 4.56 (1 \pm 0.07) \times 10^9 \text{ cm}^{-2}\text{s}^{-1} && \text{(AGSS09)}. \end{aligned} \quad (4.2)$$

The 7% uncertainty in both cases are due to the uncertainties in the cross sections of the reactions ${}^3\text{He} + {}^3\text{He} \rightarrow {}^4\text{He} + 2p$ (2.5%) and ${}^3\text{He} + {}^4\text{He} \rightarrow {}^7\text{Be} + \gamma$ (2.8%), opacity (3.2%), diffusion (2%), quoted uncertainties in the abundances (2%), and various other sources [51]. As can be seen, the central value of the flux prediction can differ considerably depending on which set of abundances are adopted. However, various predictions of the SSM based

³A kind of meteorite.

⁴ X , Y , and Z respectively denote the mass fractions of hydrogen, helium, and metals (elements other than H or He).

on the AGSS09 data set disagree with solar properties inferred from helio-seismology, while those based on GS98 show excellent agreement. (See e.g. Ref. [52] and references therein.) Thus, we will simply use the GS98 based flux for our analysis, which was also the flux used by Borexino to constrain P_{ee} [37]. The 0.862 MeV neutrinos constitute $89.56 \pm 0.04\%$ [32] of the total flux, so the GS98 prediction of $\Phi_{7\text{Be}}^{0.862}$ will be

$$\Phi_{7\text{Be}}^{0.862} = 4.48 (1 \pm 0.07) \times 10^9 \text{ cm}^{-2}\text{s}^{-1} \quad (\text{GS98}). \quad (4.3)$$

5 Uncertainties in the Mixing Angles

As discussed in section 2, we need to understand the uncertainties in $N_e \Phi_{7\text{Be}}^{0.862}$, P_{ee} , and s_{23}^2 that appear in Eq. (2.10) to constrain $\varepsilon_{\alpha L/R}$ ($\alpha = e, \tau$). In the previous sections, we have seen that N_e has an uncertainty of ${}_{-1.3}^{+0.5}\%$, while $\Phi_{7\text{Be}}^{0.862}$ has an uncertainty of $\pm 7\%$, so the uncertainty in the product $N_e \Phi_{7\text{Be}}^{0.862}$ is dominated by that in $\Phi_{7\text{Be}}^{0.862}$ and we can assign to it an uncertainty of $\pm 7\%$. Let us now look at the uncertainties in P_{ee} and s_{23}^2 .

The ν_e survival probability P_{ee} is dependent on the neutrino energy E_ν . At $E_\nu = 0.862$ MeV, matter effects are negligible and we can approximate (see, for instance, Ref. [57])

$$P_{ee} \approx 1 - \frac{1}{2} \sin^2(2\theta_{12}). \quad (5.1)$$

The best-fit values of the neutrino mixing angles from three recent global fits, Refs. [53], [54], and [55], are listed in Table 1. These analyses are more recent than what was used in the 2012 Review of Particle Properties [58], and include new results from Super-Kamiokande

Reference	Ref. [53]	Ref. [54]	Ref. [55]
$\Delta m_{21}^2 (10^{-5} \text{eV}^2)$	7.62 ± 0.19	$7.54^{+0.26}_{-0.22}$	$7.50^{+0.205}_{-0.160}$
$\Delta m_{31}^2 (10^{-3} \text{eV}^2)$ (N)	$2.55^{+0.06}_{-0.09}$	$2.43^{+0.06}_{-0.10}$	$2.49^{+0.055}_{-0.051}$
$\Delta m_{13}^2 (10^{-3} \text{eV}^2)$ (I)	$2.43^{+0.07}_{-0.06}$	$2.42^{+0.07}_{-0.11}$	$\Delta m_{23}^2 (10^{-3} \text{eV}^2) = 2.47^{+0.064}_{-0.073}$
$\sin^2 \theta_{13}$ (N)	$0.0246^{+0.0029}_{-0.0028}$	0.0241 ± 0.0025	0.025 ± 0.0023
$\sin^2 \theta_{13}$ (I)	$0.0250^{+0.0026}_{-0.0027}$	$0.0244^{+0.0023}_{-0.0025}$	
$\sin^2 \theta_{23}$ (N)	$0.427^{+0.034}_{-0.027} \oplus 0.613^{+0.022}_{-0.040}$	$0.386^{+0.024}_{-0.021}$	$0.41^{+0.030}_{-0.029} \oplus 0.60^{+0.020}_{-0.026}$
3σ range	$0.36 \rightarrow 0.68$	$0.331 \rightarrow 0.637$	$0.34 \rightarrow 0.67$
$\sin^2 \theta_{23}$ (I)	$0.600^{+0.026}_{-0.031}$	$0.392^{+0.039}_{-0.022}$	
3σ range	$0.37 \rightarrow 0.67$	$0.335 \rightarrow 0.663$	
$\sin^2 \theta_{12}$	$0.320^{+0.016}_{-0.017}$	$0.307^{+0.018}_{-0.016}$	0.31 ± 0.013
P_{ee}	$0.565^{+0.013}_{-0.011}$	0.574 ± 0.013	0.572 ± 0.010

Table 1. 1σ bounds on the neutrino mixing angles and mass-squared differences from the global fits performed in Refs. [53], [54], and [55], and the corresponding ν_e survival probability P_{ee} for the ${}^7\text{Be}$ neutrinos. N and I stand for normal and inverted hierarchies. The numbers cited from Ref. [55] are those obtained by assuming reactor neutrino fluxes of Huber [56], with the mass hierarchy marginalized for the mixing angle values. The CP violating phase δ_{CP} is essentially unconstrained so the fit values are not shown. The agreement is good for all parameters except $\sin^2 \theta_{23}$, the χ^2 of which has two local minima near 0.4 and 0.6. These minima are roughly degenerate, separated by only a minuscule ‘bump’ between them, and which one is preferred depends on the mass hierarchy and minute details of the global analyses.

[59], MINOS [60], and other experiments that were announced at the Neutrino 2012 conference in Kyoto (June 3–9, 2012).

The agreement in the values of $\sin^2 \theta_{12}$ from the three fits is good, and rounding up the resulting P_{ee} to the second decimal place yields

$$P_{ee} = 0.57 \pm 0.01 \quad (5.2)$$

for all three. We will use this value for P_{ee} in our analysis.⁵ Since the factors P_{ee} and $(1 - P_{ee})$ in Eq. (2.10) appear multiplied by the factor $N_e \Phi_{7\text{Be}}^{0.862}$ with a $\pm 7\%$ uncertainty, the small uncertainties in P_{ee} and $(1 - P_{ee})$ can be ignored.

The value of $\sin^2 \theta_{23}$ is problematic. While the new Super-Kamiokande atmospheric neutrino data still favors the maximal $\sin^2 2\theta_{23} = 1.00$ (≥ 0.94 (90% C.L.)) as the best fit value in a two-flavor oscillation analysis [59], preliminary results from MINOS prefer $\sin^2 2\theta_{23} = 0.94_{-0.05}^{+0.04}$, leading to a combined value of $\sin^2 2\theta_{23} = 0.96 \pm 0.04$ [60], which corresponds to either $\sin^2 \theta_{23} = 0.4$ or 0.6 . This degeneracy is broken in a full three flavor oscillation analysis of the atmospheric neutrino data, with the preferred value depending on the mass hierarchy [55, 59]. However, as can be seen from Table. 1, the fits of Refs. [53] and [54] do not agree on which value should be preferred over the other even when the mass hierarchy is fixed. Ref. [55] marginalizes over the mass hierarchy, so the degeneracy remains. One also needs to be aware that a small shift in the preferred value of $\sin^2 2\theta_{23}$ could shift the preferred values of $\sin^2 \theta_{23}$ considerably. So a conservative assessment of the current situation would be that the value of $\sin^2 \theta_{23}$ is somewhere in the 3σ range of $0.34 \rightarrow 0.67$ (taken from Ref. [55]), without a particularly preferred value. Thus, in this analysis, we choose to use the central $\sin^2 \theta_{23} = 0.5$ as the reference value, and associate with it an uncertainty obtained by dividing the width of the 3σ range by six:

$$s_{23}^2 = \sin^2 \theta_{23} = 0.500 \pm 0.055 . \quad (5.3)$$

That is, we associate an 11% uncertainty to s_{23}^2 .

6 Dependence of the Event Spectrum on the NSI Parameters

Before we proceed to our analysis of the Borexino 153.6 ton-year data, let us take a look at how the expected event spectrum depends on the NSI parameters to obtain a feel on which features of the spectrum are relevant in constraining which parameter.

In Fig. 1, we show the expected 153.6 ton-year Borexino event spectrum in the energy range $0.29 \text{ MeV} < T_A < 0.80 \text{ MeV}$, in 10 keV wide bins, for several choices of the NSI parameters. This energy range is dominated by the ${}^7\text{Be}$, ${}^{85}\text{Kr}$, and ${}^{210}\text{Bi}$ events, and all other solar neutrinos and background contributions can be neglected. The ${}^7\text{Be}$ signal has been calculated with inputs $\sin^2 \theta_W = 0.2386$, $P_{ee} = 0.57$, $s_{23}^2 = c_{23}^2 = 0.5$, and $\Phi_{7\text{Be}}^{0.862} = 4.48 \times 10^9 \text{ cm}^{-2}\text{s}^{-1}$, as discussed in previous sections. The total number of ${}^7\text{Be}$ counts in the shown range is 14350 for the SM case (all NSI parameters set to zero). The ${}^{85}\text{Kr}$ background has been fixed to the rate in Eq. (3.3), and the ${}^{210}\text{Bi}$ background to the

⁵The value based on the Borexino data assuming Eq. (4.3) is $P_{ee} = 0.51 \pm 0.07$ [37].

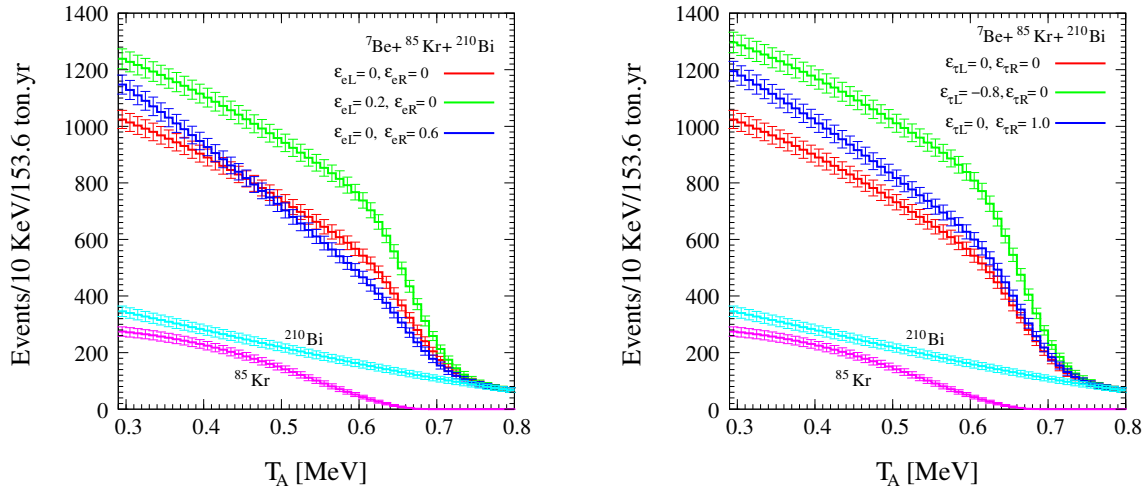


Figure 1. Expected Borexino event spectrum for a fiducial exposure of 153.6 ton-year. The numbers shown are for 10 keV wide bins, with associated statistical errors. The left-hand panel depicts the total number of events (${}^7\text{Be} + {}^{85}\text{Kr} + {}^{210}\text{Bi}$) for different choices of ε_{eL} and ε_{eR} as shown in the legends. The contributions from ${}^{85}\text{Kr}$ and ${}^{210}\text{Bi}$, which are unaffected by the NSI parameters, are also shown separately. The right-hand panel portrays the same for different choices of $\varepsilon_{\tau L}$ and $\varepsilon_{\tau R}$. Note that we have taken the sample non-zero values of the NSI parameters to be fairly large to exaggerate their effects.

rate in Eq. (3.1). The total number of counts in the range is 5813 (10057) for the ${}^{85}\text{Kr}$ (${}^{210}\text{Bi}$) background.

It is quite evident from Fig. 1 that the left-handed couplings, $\varepsilon_{\alpha L}$ ($\alpha = e, \tau$) affect the overall normalization, whereas the right-handed couplings, $\varepsilon_{\alpha R}$ ($\alpha = e, \tau$), cause changes in both shape and normalization. Thus any uncertainty in the normalization of the ${}^7\text{Be}$ signal can severely deteriorate the sensitivity to $\varepsilon_{\alpha L}$, and also mimic the presence of $\varepsilon_{\alpha R}$ to some extent. The ${}^{85}\text{Kr}$ background starts around the Compton-like edge of the ${}^7\text{Be}$ signal, and its presence affects the slope of the total event spectrum below this edge in a way similar to non-zero values of $\varepsilon_{\alpha R}$. Thus, the uncertainty in this background can be expected to deteriorate the sensitivity to $\varepsilon_{\alpha R}$. Note also that the events above the ${}^7\text{Be}$ Compton-like edge, $0.7 \text{ MeV} \lesssim T_A$, are dominated by the ${}^{210}\text{Bi}$ background as discussed previously, so this background will be constrained by the events in this region when performing a fit.

To see how the uncertainties in the normalization of the ${}^7\text{Be}$ signal and the ${}^{85}\text{Kr}$ background could affect the bounds on the NSI parameters, we perform the following analysis. Let N_i^{th} be the expected number of events in the i -th energy bin. Construct the χ^2 by

$$\chi^2(\varepsilon_{\alpha C}, \Delta N_X) = \sum_i \frac{[N_i^{\text{th}}(0, 0) - N_i^{\text{th}}(\varepsilon_{\alpha C}, \Delta N_X)]^2}{N_i^{\text{th}}(0, 0)}, \quad \alpha = e \text{ or } \tau, \quad (6.1)$$

where $C = L$ or R , and $X = \text{Be}$ or Kr . ΔN_{Be} and ΔN_{Kr} are respectively the percentage changes in the normalizations of the ${}^7\text{Be}$ signal and ${}^{85}\text{Kr}$ background from their reference values. Implicit parameters are all fixed to the reference values we used above. This χ^2

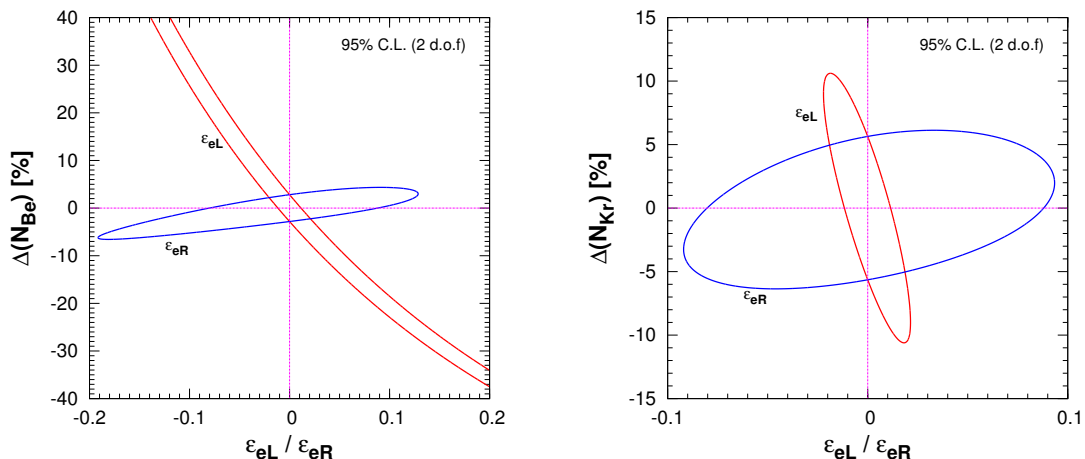


Figure 2. Correlations between the NSI parameters and the normalizations of the ${}^7\text{Be}$ signal and ${}^{85}\text{Kr}$ background. The left-hand panel shows the 95% C.L. contours (2 d.o.f., $\Delta\chi^2 = 5.99$) in the $\Delta N_{\text{Be}}-\varepsilon_{eL,R}$ plane, while the right-hand panel shows the same in the $\Delta N_{\text{Kr}}-\varepsilon_{eL,R}$ plane. The area inside the contours are allowed. All implicit parameters are set to their reference values used in Fig. 1.

quantifies the ability of Borexino to distinguish between the $(\varepsilon_{\alpha C}, \Delta N_X) = (0, 0)$ and non-zero cases. Using this χ^2 for the case $\alpha = e$, we plot the 95% C.L. contours ($\Delta\chi^2 = 5.99$) in the $\Delta N_X-\varepsilon_{eC}$ planes in Fig. 2.

The left-hand panel of Fig. 2 shows the correlations between $\varepsilon_{eL/R}$ and ΔN_{Be} . For ε_{eL} , we can see that it has a strong negative correlation to ΔN_{Be} , as was expected from our discussion above. Thus, a large uncertainty in ΔN_{Be} would lead to a large uncertainty in ε_{eL} . ε_{eR} , on the other hand, is only weakly correlated with ΔN_{Be} , again as expected.

The right-hand panel of Fig. 2 shows the correlations between $\varepsilon_{eL/R}$ and ΔN_{Kr} . For ε_{eL} , we see that it is only weakly correlated with ΔN_{Kr} as expected. ε_{eR} , however, is also only weakly correlated with ΔN_{Kr} somewhat contrary to expectation. Consequently, a reduction in the uncertainty of ΔN_{Kr} will not lead to any significant reduction in the uncertainty of ε_{eR} . In the following, we will find that the reduction of the ${}^{85}\text{Kr}$ background itself, and not just its uncertainty, is necessary to improve the bound on ε_{eR} .

7 Analysis Results

7.1 Method of Analysis

Let us now proceed to our analysis of the Borexino 153.6 ton-year data. As in the previous section, we consider events in the energy range $0.29 \text{ MeV} < T_A < 0.80 \text{ MeV}$, which we divide into 10 keV bins.

Let the number of measured counts in the i -th bin be N_i^{exp} , and its theoretical value $N_i^{\text{th}}(\vec{\lambda})$, where $\vec{\lambda}$ denotes the fit parameters that will be varied:

$$\vec{\lambda} = \{ \varepsilon_{eL}, \varepsilon_{eR}, \varepsilon_{\tau L}, \varepsilon_{\tau R}, \Delta N_{\text{Be}}, \Delta N_{\text{Kr}}, \Delta N_{\text{Bi}}, s_{23}^2 \}. \quad (7.1)$$

	ε_{eL}	ε_{eR}	$\varepsilon_{\tau L}$	$\varepsilon_{\tau R}$
This work	[-0.046, 0.053]	[-0.206, 0.157]	[-0.231, 0.866]	[-0.976, 0.726]
Global limits [18]	[-0.03, 0.08]	[0.004, 0.151]	[-0.5, 0.2]	[-0.3, 0.4]

Table 2. The 90% C.L. limits on the flavor-diagonal NSI parameters ε_{eL} , ε_{eR} , $\varepsilon_{\tau L}$ and $\varepsilon_{\tau R}$ based on 153.6 ton-years of Borexino data. In each case, only one NSI parameter and the three normalization parameters are allowed to float, while the remaining three NSI parameters are fixed to zero. The three normalization parameters are marginalized to obtain these bounds. The second row lists the global bounds from Ref. [18] for comparison.

ΔN_{Be} , ΔN_{Kr} and ΔN_{Bi} respectively denote the percentage change in the ${}^7\text{Be}$, ${}^{85}\text{Kr}$, and ${}^{210}\text{Bi}$ event normalizations from their reference values. The first is varied to account for the $\pm 7\%$ uncertainty in the ${}^7\text{Be}$ neutrino flux, while the second for the $\pm 18\%$ uncertainty in the ${}^{85}\text{Kr}$ background, c.f. Eq. (3.3). s_{23}^2 is varied with a $\pm 11\%$ uncertainty around the reference value of 0.5 as discussed in section 5. The χ^2 is then defined as

$$\chi^2(\vec{\lambda}) = \sum_i \frac{[N_i^{\text{exp}} - N_i^{\text{th}}(\vec{\lambda})]^2}{N_i^{\text{exp}}} + \left[\frac{\Delta N_{\text{Be}}}{7\%} \right]^2 + \left[\frac{\Delta N_{\text{Kr}}}{18\%} \right]^2 + \left(\frac{s_{23}^2 - 0.5}{0.055} \right)^2. \quad (7.2)$$

No prior constraint is imposed on ΔN_{Bi} , which will be left for the fit to determine.

Since we do not have access to the raw 153.6 ton-year Borexino data, we reconstruct the counts N_i^{exp} from the fits listed in Eq. (3.1) as a sum of ${}^7\text{Be}$, ${}^{85}\text{Kr}$, and ${}^{210}\text{Bi}$ events. Contributions from other solar neutrinos and backgrounds are neglected. The theoretical value $N_i^{\text{th}}(\vec{\lambda})$ is calculated with the parameter selection used in the previous section. Note that N_i^{exp} is not equal to $N_i^{\text{th}}(\vec{0})$. Thus, the minimal value of χ^2 will be non-zero:

$$\chi^2(\vec{\lambda}) = \chi_{\text{min}}^2 + \Delta\chi^2(\vec{\lambda}). \quad (7.3)$$

Using this $\Delta\chi^2$, we first place constraints on the four NSI parameters one at a time, keeping the other three NSI parameters zero, while marginalizing⁶ over the three normalization parameters and s_{23}^2 . Then, we place constraints on pairs of NSI parameters, one flavor at a time, keeping the other flavor pair zero, while again marginalizing over the normalization parameters and s_{23}^2 .

7.2 One NSI parameter at a time limits

The dependence of $\Delta\chi^2$ on one NSI parameter, with the other three fixed to zero, and after marginalization of the three normalization parameters, is shown in Fig. 3 for all four choices of the NSI parameter. The corresponding 90% C.L. limits (1 d.o.f, $\Delta\chi^2 = 2.71$) are listed in Table 2, together with the global fit values from Ref. [18] for comparison. We can see that the bounds based on Borexino data alone is already competitive with the global fit to reactor+accelerator data.

⁶For a discussion on the ‘marginalization’ procedure see, for instance, Refs. [61] and [62].

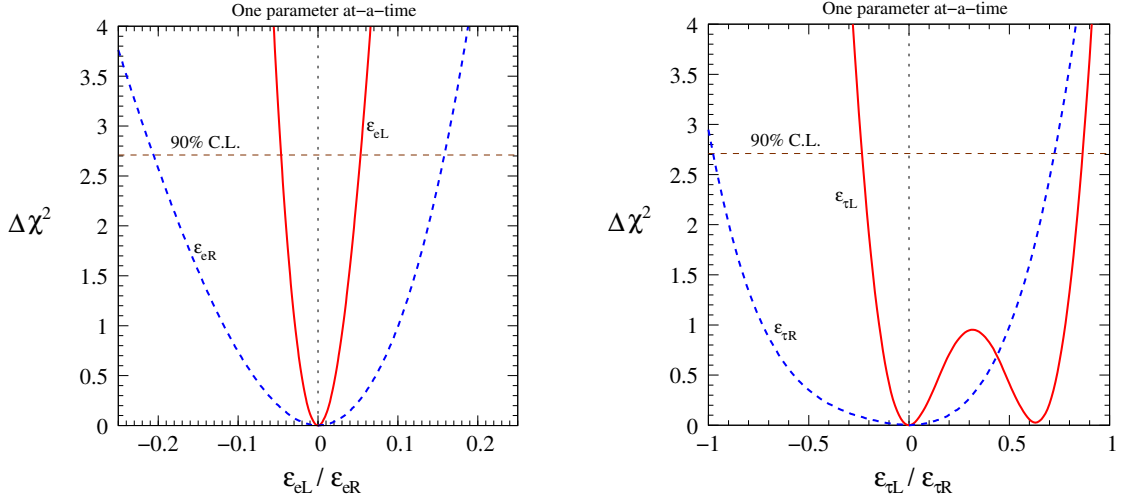


Figure 3. Left-hand panel depicts the one NSI parameter at a time limit for ϵ_{eL} and ϵ_{eR} . Right-hand panel shows the same for $\epsilon_{\tau L}$ and $\epsilon_{\tau R}$. The corresponding limits at 90% C.L. (1 d.o.f, $\Delta\chi^2 = 2.71$) are listed in Table 2. The central values of the NSI parameters are zero despite our using the value $P_{ee} = 0.57$ in our reference model instead of $P_{ee} = 0.51$ preferred by the Borexino data, since the discrepancy is absorbed into the uncertainty in the ${}^7\text{Be}$ flux.

Since July 2010, the Borexino experiment have undertaken a series of purification campaigns to reduce the radioactive backgrounds. The method of Nitrogen stripping has been quite successful in reducing the ${}^{85}\text{Kr}$ background to roughly 30% of previous levels [63]. In 2012, with these lower backgrounds, the Borexino experiment has entered into its Phase II run and continues to accumulate more data.

Let us quantify the expected improvements on the NSI bounds due to improved statistics and the reduction of the ${}^{85}\text{Kr}$ background. In the leftmost panel of Fig. 4, we show how the bounds on the electron NSI parameters ϵ_{eL} and ϵ_{eR} will be affected by an increase in the total fiducial exposure while keeping all other assumptions the same. The vertical dot-dashed line indicates the current fiducial exposure of 153.6 ton-years. The leftmost panel of Fig. 5 shows the same for the tau NSI parameters $\epsilon_{\tau L}$ and $\epsilon_{\tau R}$. We can see from these panels that increased statistics will not improve the limits on the left-handed coupling at all, while the improvements in the right-handed couplings are quite modest, indicating that the current uncertainties in the NSI parameters are mostly due to backgrounds and systematic uncertainties.

In the center panel of Fig. 4, we show the impact of a reduction in the ${}^{85}\text{Kr}$ background on the bounds on ϵ_{eL} and ϵ_{eR} , with a fixed fiducial exposure of 153.6 ton-years. The reduction is expressed in percentages compared to Eq. (3.3). The center panel of Fig. 5 shows the same for $\epsilon_{\tau L}$ and $\epsilon_{\tau R}$. As discussed in section 6, we expect the bounds on the left-handed couplings, which change the ${}^7\text{Be}$ signal normalization, to be little affected since the ${}^{85}\text{Kr}$ background mostly changes the slope of the spectrum, and indeed the figures confirm this expectation. The bounds on the right-handed couplings, on the other hand, can be tightened. If the ${}^{85}\text{Kr}$ background is reduced down to 10%, the bounds on ϵ_{eR} will

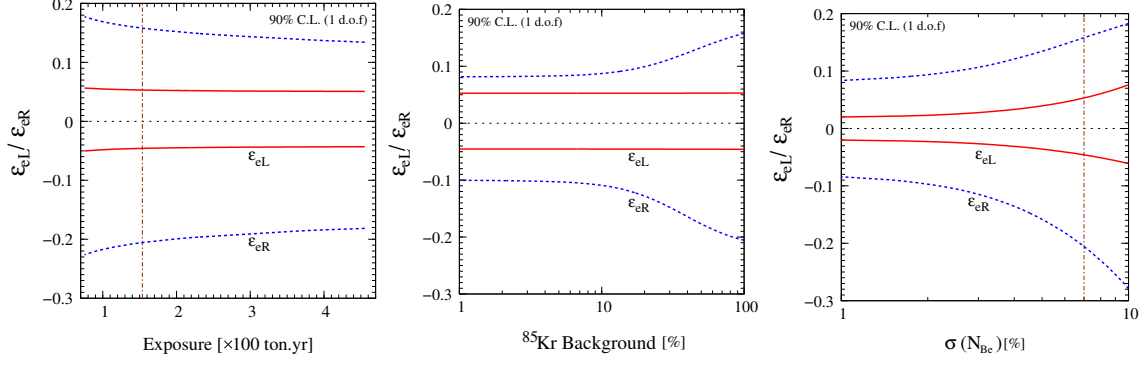


Figure 4. One NSI parameter at a time limits on ε_{eL} and ε_{eR} at 90% C.L. (1 d.o.f) as a function of total fiducial exposure (left panel), total amount of ^{85}Kr background (middle panel), and 1σ uncertainty on ^7Be signal rate (right panel).

shrink by a factor of ~ 2 , while those on $\varepsilon_{\tau R}$ will shrink by a factor of ~ 1.5 .

In the rightmost panels of Figs. 4 and 5, we show the impact of a reduction in the uncertainty of the ^7Be signal normalization on the bounds on ε_{eL} and ε_{eR} , and $\varepsilon_{\tau L}$ and $\varepsilon_{\tau R}$, respectively. All other assumptions, including the fiducial exposure of 153.6 ton-years, are kept the same. The vertical dot-dashed lines show the current 1σ uncertainty of $\pm 7\%$. If we can reduce this uncertainty from 7% to, say, 3% then for ε_{eL} and ε_{eR} , the limits can be improved roughly by a factor of 1.5. For $\varepsilon_{\tau L}$, we find two disjoint regions if we can go below 3%. Such an improvement must first follow the resolution of the solar metallicity problem we alluded to in section 4, and further improvements in nuclear cross section measurements.

7.3 Constraints in the $(\varepsilon_{eL}-\varepsilon_{eR})$ and $(\varepsilon_{\tau L}-\varepsilon_{\tau R})$ planes

Let us now turn to 2D constraints in the left-right coupling plane of each flavor. In Fig. 6, we show the allowed regions in the $(\varepsilon_{eL}-\varepsilon_{eR})$ plane at 95% C.L. (2 d.o.f, $\Delta\chi^2 = 5.99$), obtained with the τ NSI parameters set to zero, $\varepsilon_{\tau L} = \varepsilon_{\tau R} = 0$, and the normalization

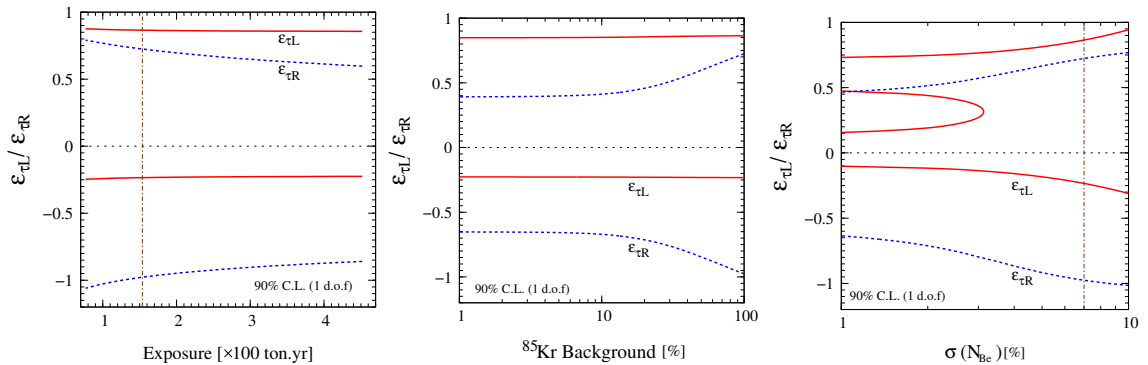


Figure 5. One NSI parameter at a time limits on $\varepsilon_{\tau L}$ and $\varepsilon_{\tau R}$ at 90% C.L. (1 d.o.f) as a function of total fiducial exposure (left panel), total amount of ^{85}Kr background (middle panel), and 1σ uncertainty on ^7Be signal rate (right panel).

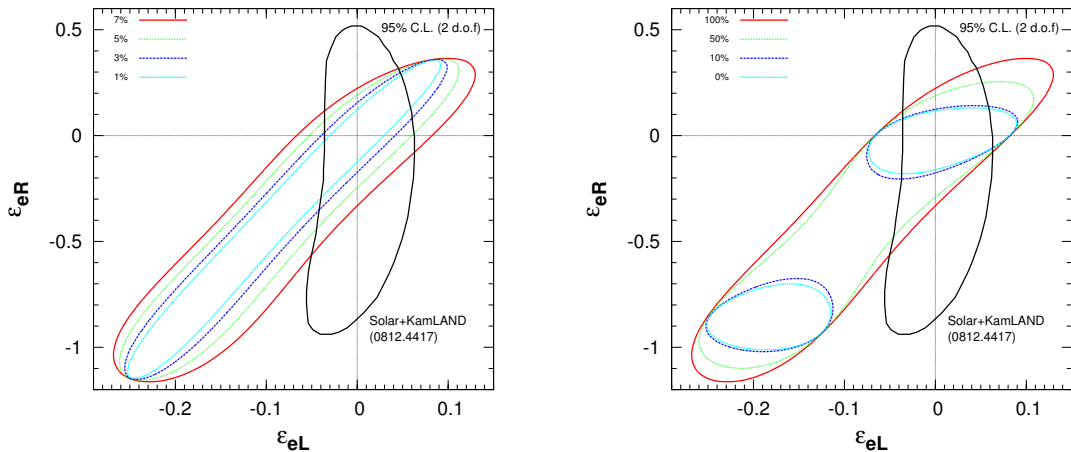


Figure 6. Allowed regions in the ε_{eL} - ε_{eR} plane at 95% C.L. (2 d.o.f, $\Delta\chi^2 = 5.99$). In this analysis, $\varepsilon_{\tau L}$ and $\varepsilon_{\tau R}$ are fixed to zero, while the normalization parameters and s_{23}^2 are marginalized. The solid red curves indicate the current bounds, while the green, blue, and cyan curves indicate what the bounds would be with reduced uncertainty in the ${}^7\text{Be}$ signal normalization (left-panel), and reduced ${}^{85}\text{Kr}$ background (right-panel). The area outside each contour is excluded. The bound from Ref. [17] is plotted in black for comparison.

parameters and s_{23}^2 marginalized. On both panels, the solid red curves indicate the current bounds with 153.6 ton·year fiducial exposure, 7% uncertainty in the normalization of the ${}^7\text{Be}$ signal, and with the full ${}^{85}\text{Kr}$ background. On the left-hand panel, three more curves indicate the bounds assuming three different uncertainty levels (see legends in the figure) in the ${}^7\text{Be}$ signal normalization. On the right-hand panel, three more curves indicate the bounds with three different assumptions (see legends in the figure) on the amount of ${}^{85}\text{Kr}$ background. For comparison, we plot the combined solar+KamLAND bound obtained in Ref. [17] in black. In Fig. 7, we show the same for the $(\varepsilon_{\tau L}$ - $\varepsilon_{\tau R})$ plane. For comparison, the bound based on the LEP ‘neutrino counting’ data [18] is plotted in black.

Here, we find that the Borexino bounds are comparable in size to those from Ref. [17] and [18], but occupy slightly different regions in the 2D parameter space. Thus, the overlap region in 2D is smaller than either Borexino, or the reference bounds alone. While the expected improvements to the bounds due to reduced normalization uncertainty and ${}^{85}\text{Kr}$ background are modest for the τ -parameters, they can be considerable for the electron parameters, particularly if the ${}^{85}\text{Kr}$ background can be reduced to 10% of previous levels.

8 Summary

We have used the 153.6 ton·year fiducial exposure data from Borexino to place bounds on the flavor-diagonal NSI parameters ε_{eL} , ε_{eR} , $\varepsilon_{\tau L}$, and $\varepsilon_{\tau R}$ taking into account the $\pm 7\%$ uncertainty in the ${}^7\text{Be}$ solar neutrino flux, $\Phi_{7\text{Be}}^{0.862}$, and the backgrounds from ${}^{85}\text{Kr}$ and ${}^{210}\text{Bi}$ β -decay. The uncertainty in $\sin^2 \theta_{23}$ was assumed to be $\pm 11\%$ around the reference value of 0.5. The resulting one NSI parameter at a time bounds are listed in Table 2. 2D bounds

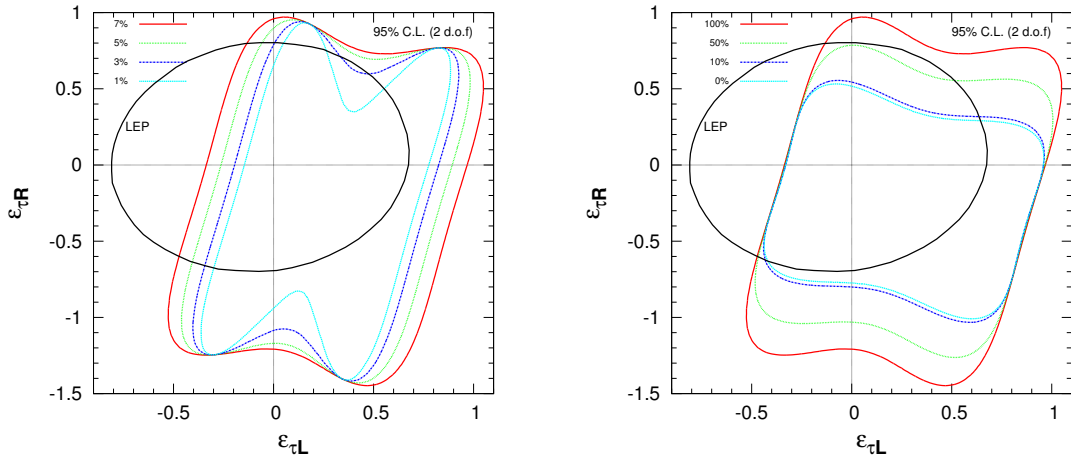


Figure 7. Allowed regions in the $\varepsilon_{\tau L}$ - $\varepsilon_{\tau R}$ plane at 95% C.L. (2 d.o.f, $\Delta\chi^2 = 5.99$). In this analysis, ε_{eL} and ε_{eR} are fixed to zero, while the normalization parameters are marginalized. The solid red curves indicate the current bounds, while the green, blue, and cyan curves indicate what the bounds would be with reduced uncertainty in the ${}^7\text{Be}$ signal normalization (left-panel), and reduced ${}^{85}\text{Kr}$ background (right-panel). The area outside each contour is excluded. The bound from Ref. [18] is plotted in black for comparison.

in the $(\varepsilon_{eL}-\varepsilon_{eR})$ and $(\varepsilon_{\tau L}-\varepsilon_{\tau R})$ planes are shown in figures 6 and 7. They are comparable to existing bounds in Ref. [17] and [18].

Further improvements in the bounds would require reductions in the ${}^{85}\text{Kr}$ background, which is already underway in Borexino Phase II, and in the uncertainty of the ${}^7\text{Be}$ solar neutrino flux. The latter may be achieved by the resolution of the solar metallicity problem, and improvements in the relevant cross section measurements by future experiments such as DIANA [64].

Acknowledgments

We would like to thank Carlos Peña-Garay, Patrick Huber, Jonathan Link, and Bruce Vogelaar for helpful discussions. We would also like to thank Yee Kao for his contributions to the early stages of this work. TT is grateful for the hospitality of the Instituto de Física Corpuscular (IFIC) at the University of Valencia, Spain, where a large portion of this work was carried out during his visit in June 2012. SKA acknowledges the support from the European Union under the European Commission FP7 Research Infrastructure Design Studies EUROnu (Grant Agreement No. 212372 FP7-INFRA-2007-1), LAGUNA (Grant Agreement No. 212343 FP7-INFRA-2007-1), and the project Consolider-Ingenio CUP. FL is supported by the Università degli Studi dell’Aquila, Dipartimento di Fisica, and by a PhD scholarship from the Laboratori Nazionali del Gran Sasso (INFN-LNGS). TT is supported in part by the U.S. Department of Energy, grant DE-FG05-92ER40677, task A.

References

- [1] E. Roulet, *MSW effect with flavor changing neutrino interactions*, *Phys.Rev.* **D44** (1991) 935–938.
- [2] M. Guzzo, A. Masiero, and S. Petcov, *On the MSW effect with massless neutrinos and no mixing in the vacuum*, *Phys.Lett.* **B260** (1991) 154–160.
- [3] V. D. Barger, R. Phillips, and K. Whisnant, *Solar neutrino solutions with matter enhanced flavor changing neutral current scattering*, *Phys.Rev.* **D44** (1991) 1629–1643.
- [4] S. Bergmann and Y. Grossman, *Can lepton flavor violating interactions explain the LSND results?*, *Phys.Rev.* **D59** (1999) 093005, [[hep-ph/9809524](#)].
- [5] S. Bergmann, Y. Grossman, and D. M. Pierce, *Can lepton flavor violating interactions explain the atmospheric neutrino problem?*, *Phys.Rev.* **D61** (2000) 053005, [[hep-ph/9909390](#)].
- [6] S. Antusch, J. P. Baumann, and E. Fernandez-Martinez, *Non-Standard Neutrino Interactions with Matter from Physics Beyond the Standard Model*, *Nucl.Phys.* **B810** (2009) 369–388, [[arXiv:0807.1003](#)].
- [7] M. Gavela, D. Hernandez, T. Ota, and W. Winter, *Large gauge invariant non-standard neutrino interactions*, *Phys.Rev.* **D79** (2009) 013007, [[arXiv:0809.3451](#)].
- [8] M. Malinsky, T. Ohlsson, and H. Zhang, *Non-Standard Neutrino Interactions from a Triplet Seesaw Model*, *Phys.Rev.* **D79** (2009) 011301, [[arXiv:0811.3346](#)].
- [9] T. Ohlsson, T. Schwetz, and H. Zhang, *Non-standard neutrino interactions in the Zee-Babu model*, *Phys.Lett.* **B681** (2009) 269–275, [[arXiv:0909.0455](#)].
- [10] M. Medina and P. de Holanda, *Non-standard neutrinos interactions in a 331 model with minimum Higgs sector*, *Adv.High Energy Phys.* **2012** (2012) 763829, [[arXiv:1108.5228](#)].
- [11] Z. Berezhiani and A. Rossi, *Limits on the nonstandard interactions of neutrinos from $e+e-$ colliders*, *Phys.Lett.* **B535** (2002) 207–218, [[hep-ph/0111137](#)].
- [12] Z. Berezhiani, R. Raghavan, and A. Rossi, *Probing nonstandard couplings of neutrinos at the Borexino detector*, *Nucl.Phys.* **B638** (2002) 62–80, [[hep-ph/0111138](#)].
- [13] Z. G. Berezhiani and A. Rossi, *Vacuum oscillation solution to the solar neutrino problem in standard and nonstandard pictures*, *Phys.Rev.* **D51** (1995) 5229–5239, [[hep-ph/9409464](#)].
- [14] S. Davidson, C. Pena-Garay, N. Rius, and A. Santamaria, *Present and future bounds on nonstandard neutrino interactions*, *JHEP* **0303** (2003) 011, [[hep-ph/0302093](#)].
- [15] **CHARM-II** Collaboration, P. Vilain et al., *Precision measurement of electroweak parameters from the scattering of muon-neutrinos on electrons*, *Phys.Lett.* **B335** (1994) 246–252.
- [16] J. Barranco, O. Miranda, C. Moura, and J. Valle, *Constraining non-standard interactions in $\nu(e)e$ or $\bar{\nu}(e)e$ scattering*, *Phys.Rev.* **D73** (2006) 113001, [[hep-ph/0512195](#)].
- [17] A. Bolanos, O. Miranda, A. Palazzo, M. Tortola, and J. Valle, *Probing non-standard neutrino-electron interactions with solar and reactor neutrinos*, *Phys.Rev.* **D79** (2009) 113012, [[arXiv:0812.4417](#)].
- [18] J. Barranco, O. Miranda, C. Moura, and J. Valle, *Constraining non-standard neutrino-electron interactions*, *Phys.Rev.* **D77** (2008) 093014, [[arXiv:0711.0698](#)].

- [19] **ALEPH Collaboration, DELPHI Collaboration, L3 Collaboration, OPAL Collaboration, SLD Collaboration, LEP Electroweak Working Group, SLD Electroweak Group, SLD Heavy Flavour Group** Collaboration, *Precision electroweak measurements on the Z resonance*, *Phys.Rept.* **427** (2006) 257–454, [[hep-ex/0509008](#)].
- [20] **LSND Collaboration**, L. Auerbach et al., *Measurement of electron - neutrino - electron elastic scattering*, *Phys.Rev.* **D63** (2001) 112001, [[hep-ex/0101039](#)].
- [21] F. Reines, H. Gurr, and H. Sobel, *Detection of anti-electron-neutrino e Scattering*, *Phys.Rev.Lett.* **37** (1976) 315–318.
- [22] A. Derbin, A. Chernyi, L. Popeko, V. Muratova, G. Shishkina, et al., *Experiment on anti-neutrino scattering by electrons at a reactor of the Rovno nuclear power plant*, *JETP Lett.* **57** (1993) 768–772.
- [23] **MUNU Collaboration**, Z. Daraktchieva et al., *Limits on the neutrino magnetic moment from the MUNU experiment*, *Phys.Lett.* **B564** (2003) 190–198, [[hep-ex/0304011](#)].
- [24] C. Biggio, M. Blennow, and E. Fernandez-Martinez, *Loop bounds on non-standard neutrino interactions*, *JHEP* **0903** (2009) 139, [[arXiv:0902.0607](#)].
- [25] C. Biggio, M. Blennow, and E. Fernandez-Martinez, *General bounds on non-standard neutrino interactions*, *JHEP* **0908** (2009) 090, [[arXiv:0907.0097](#)].
- [26] A. Friedland, C. Lunardini, and M. Maltoni, *Atmospheric neutrinos as probes of neutrino-matter interactions*, *Phys.Rev.* **D70** (2004) 111301, [[hep-ph/0408264](#)].
- [27] A. Friedland and C. Lunardini, *Two modes of searching for new neutrino interactions at MINOS*, *Phys.Rev.* **D74** (2006) 033012, [[hep-ph/0606101](#)].
- [28] **TEXONO Collaboration**, M. Deniz et al., *Constraints on Non-Standard Neutrino Interactions and Unparticle Physics with Neutrino-Electron Scattering at the Kuo-Sheng Nuclear Power Reactor*, *Phys.Rev.* **D82** (2010) 033004, [[arXiv:1006.1947](#)].
- [29] J. Erler and P. Langacker, “Electroweak model and constraints on new physics.” in Ref. [58].
- [30] S. K. Agarwalla and P. Huber, *Potential measurement of the weak mixing angle with neutrino-electron scattering at low energy*, *JHEP* **1108** (2011) 059, [[arXiv:1005.1254](#)].
- [31] P. Vogel and J. Engel, *Neutrino Electromagnetic Form-Factors*, *Phys.Rev.* **D39** (1989) 3378.
- [32] D. Tilley, C. Cheves, J. Godwin, G. Hale, H. Hofmann, et al., *Energy levels of light nuclei A=5, A=6, A=7*, *Nucl.Phys.* **A708** (2002) 3–163.
- [33] **Borexino Collaboration**, G. Bellini et al., *The Borexino experiment and the results of the Counting Test Facility*, *Nucl.Phys.Proc.Suppl.* **48** (1996) 363–369.
- [34] **Borexino Collaboration**, H. Back et al., *Pulse-shape discrimination with the counting test facility*, *Nucl.Instrum.Meth.* **A584** (2008) 98–113, [[arXiv:0705.0239](#)].
- [35] **Borexino Collaboration**, C. Arpesella et al., *First real time detection of Be-7 solar neutrinos by Borexino*, *Phys.Lett.* **B658** (2008) 101–108, [[arXiv:0708.2251](#)].
- [36] **Borexino Collaboration**, C. Arpesella et al., *Direct Measurement of the Be-7 Solar Neutrino Flux with 192 Days of Borexino Data*, *Phys.Rev.Lett.* **101** (2008) 091302, [[arXiv:0805.3843](#)].
- [37] G. Bellini, J. Benziger, D. Bick, S. Bonetti, G. Bonfini, et al., *Precision measurement of the ^7Be solar neutrino interaction rate in Borexino*, *Phys.Rev.Lett.* **107** (2011) 141302, [[arXiv:1104.1816](#)].

- [38] **Borexino** Collaboration, G. Alimonti et al., *The Borexino detector at the Laboratori Nazionali del Gran Sasso*, *Nucl.Instrum.Meth.* **A600** (2009) 568–593, [[arXiv:0806.2400](#)].
- [39] **Borexino** Collaboration, G. Alimonti et al., *Measurement of the C-14 abundance in a low-background liquid scintillator*, *Phys.Lett.* **B422** (1998) 349–358.
- [40] C. Galbiati, A. Pocar, D. Franco, A. Ianni, L. Cadonati, et al., *Cosmogenic C-11 production and sensitivity of organic scintillator detectors to pep and CNO neutrinos*, *Phys.Rev.* **C71** (2005) 055805, [[hep-ph/0411002](#)].
- [41] A. Ianni, *Maximum-likelihood analysis and goodness-of-fit estimation in low count-rate experiments: Kr-85 beta activity in the test facility of the Borexino detector and double-beta decay of Ge-76 in the Heidelberg-Moscow experiment*, *Nucl.Instrum.Meth.* **A516** (2004) 184–192.
- [42] F. Villante, A. Ianni, F. Lombardi, G. Pagliaroli, and F. Vissani, *A Step toward CNO solar neutrinos detection in liquid scintillators*, *Phys.Lett.* **B701** (2011) 336–341, [[arXiv:1104.1335](#)].
- [43] **Borexino** Collaboration, G. Bellini et al., *First evidence of pep solar neutrinos by direct detection in Borexino*, *Phys.Rev.Lett.* **108** (2012) 051302, [[arXiv:1110.3230](#)].
- [44] J. N. Bahcall and M. Pinsonneault, *What do we (not) know theoretically about solar neutrino fluxes?*, *Phys.Rev.Lett.* **92** (2004) 121301, [[astro-ph/0402114](#)].
- [45] **LUNA** Collaboration, F. Confortola et al., *Astrophysical S-factor of the He-3(alpha,gamma)Be-7 reaction measured at low energy via prompt and delayed gamma detection*, *Phys.Rev.* **C75** (2007) 065803, [[arXiv:0705.2151](#)].
- [46] **LUNA** Collaboration, H. Costantini, D. Bemmerer, F. Confortola, A. Formicola, G. Gyurky, et al., *The He-3(alpha,gamma)Be-7 S-factor at solar energies: The Prompt gamma experiment at LUNA*, *Nucl.Phys.* **A814** (2008) 144–158, [[arXiv:0809.5269](#)].
- [47] C. Pena-Garay and A. Serenelli, *Solar neutrinos and the solar composition problem*, [arXiv:0811.2424](#).
- [48] N. Grevesse and A. J. Sauval, *Standard Solar Composition*, *Space Sci.Rev.* **85** (1998) 161–174.
- [49] M. Asplund, N. Grevesse, A. J. Sauval, and P. Scott, *The chemical composition of the Sun*, *Ann.Rev.Astron.Astrophys.* **47** (2009) 481–522, [[arXiv:0909.0948](#)].
- [50] A. M. Serenelli, W. Haxton, and C. Pena-Garay, *Solar models with accretion. I. Application to the solar abundance problem*, *Astrophys.J.* **743** (2011) 24, [[arXiv:1104.1639](#)].
- [51] C. Pena-Garay, *Solar neutrinos and the solar composition*, 2009. Talk given at the Workshop on Neutrino Telescopes, March 10-13, 2009, Venice, Italy, <http://neutrino.pd.infn.it/NEUTEL09/>.
- [52] A. Serenelli, *Solar neutrinos and the sun*, [arXiv:1109.2602](#).
- [53] D. Forero, M. Tortola, and J. Valle, *Global status of neutrino oscillation parameters after Neutrino-2012*, [arXiv:1205.4018](#).
- [54] G. Fogli, E. Lisi, A. Marrone, D. Montanino, A. Palazzo, et al., *Global analysis of neutrino masses, mixings and phases: entering the era of leptonic CP violation searches*, *Phys.Rev.* **D86** (2012) 013012, [[arXiv:1205.5254](#)].

- [55] M. Gonzalez-Garcia, M. Maltoni, J. Salvado, and T. Schwetz, *Global fit to three neutrino mixing: critical look at present precision*, [arXiv:1209.3023](https://arxiv.org/abs/1209.3023).
- [56] P. Huber, *On the determination of anti-neutrino spectra from nuclear reactors*, *Phys.Rev.* **C84** (2011) 024617, [[arXiv:1106.0687](https://arxiv.org/abs/1106.0687)].
- [57] K. Nakamura and S. T. Petkov, “Neutrino mass, mixing, and oscillations.” in Ref. [58].
- [58] **Particle Data Group** Collaboration, J. Beringer et al., *Review of particle physics*, *Phys.Rev.* **D86** (2012) 010001.
- [59] Y. Itow, *Atmospheric neutrinos: Results from running experiments*, 2012. Talk given at the Neutrino 2012 Conference, June 3-9, 2012, Kyoto, Japan, <http://neu2012.kek.jp/>.
- [60] **MINOS** Collaboration, R. Nichol, *Final minos results*, 2012. Talk given at the Neutrino 2012 Conference, June 3-9, 2012, Kyoto, Japan, <http://neu2012.kek.jp/>.
- [61] P. Huber, M. Lindner, and W. Winter, *Superbeams versus neutrino factories*, *Nucl.Phys.* **B645** (2002) 3–48, [[hep-ph/0204352](https://arxiv.org/abs/hep-ph/0204352)].
- [62] G. Fogli, E. Lisi, A. Marrone, D. Montanino, A. Palazzo, et al., *Solar neutrino oscillation parameters after first KamLAND results*, *Phys.Rev.* **D67** (2003) 073002, [[hep-ph/0212127](https://arxiv.org/abs/hep-ph/0212127)].
- [63] **Borexino** Collaboration, M. Pallavicini, *Results and perspectives of borexino*, 2012. Talk given at the Neutrino 2012 Conference, June 3-9, 2012, Kyoto, Japan, <http://neu2012.kek.jp/>.
- [64] **DIANA** Collaboration, D. Leitner, M. Leitner, and P. Vetter, *Diana, a novel nuclear astrophysics underground accelerator facility*, . <http://ecrgroup.lbl.gov/DIANA.htm>.